# Ion Concentration Polarization Causes a Nearly Pore-Length-Independent Conductance of Nanopores

DaVante Cain,<sup>1</sup> Ethan Cao,<sup>1</sup> Ivan Vlassiouk,<sup>2</sup> Tilman E. Schäffer,<sup>3\*</sup> Zuzanna S. Siwy<sup>1\*</sup>

<sup>1</sup>Department of Physics and Astronomy, University of California, Irvine, California, 92697, USA

<sup>2</sup>Center for Nanophase Materials Sciences, Oak Ridge National Laboratory, Oak Ridge, TN, 37831 USA

<sup>3</sup>Institute of Applied Physics, University of Tübingen, 72076 Tübingen, Germany

### Abstract

There has been a great amount of interest in nanopores as the basis for sensors and templates for preparation of biomimetic channels as well as model systems to understand transport properties at the nanoscale. The presence of surface charges on the pore walls has been shown to induce ion selectivity as well as enhance ionic conductance compared to uncharged pores. Here, using three-dimensional continuum modeling, we examine the role of length of charged nanopores as well as applied voltage for controlling ion selectivity and ionic conductance of single nanopores and small nanopore arrays. First, we present conditions where the ion current and ion selectivity of nanopores with homogeneous surface charges remain unchanged even if the pore length decreases by a factor of 6. This length-independent conductance is explained through the effect of ion concentration polarization (ICP) that modifies local ionic concentrations not only at the pore entrances but also in the pore in a voltage-dependent manner. We describe how voltage controls ion selectivity of nanopores with different lengths and present conditions when charged nanopores conduct less current than uncharged pores of the same geometrical characteristics. The manuscript provides different measures of the extent of the depletion zone induced by ICP in single pores and nanopore arrays including systems with ionic diodes. The modeling shown here will help design selective nanopores for a variety of applications where single nanopores and nanopore arrays are used.

<sup>\*</sup> Corresponding Authors: tilman.schaeffer@uni-tuebingen.de, zsiwy@uci.edu

### Introduction

The presence of surface charges in nanopores is the basis for ion selectivity such that pores with negative/positive surface charges were shown to be filled predominantly with cations/anions if the pore radius is comparable to the Debye screening length. Consequently, when an electric field is applied, the current will be carried predominantly by one type of charge carriers. Recent modeling work showed, however, that such ion selectivity decreases when the pore length approaches the pore diameter, especially if the membrane surfaces remain uncharged. To achieve ion selectivity and high ion conductance it is therefore necessary to optimize not only the pore diameter but also the pore length.

lon selectivity of nanopores has become an important topic since the demonstration that selective nanopores can be applied for osmotic energy conversion. <sup>13-15</sup> In that set-up, an ion selective pore is in contact with a salt concentration gradient, such as between fresh water in a river and salt water from a sea. <sup>16</sup> The observed electric potential difference that develops across the membrane is capped by the Nernst-potential. Several single nanopore systems were reported to exhibit high osmotic energy conversion bringing hope for 'blue' energy. <sup>13, 14, 16-18</sup> Short pores feature high conductance but when arranged in nanopore arrays the effect of ion concentration polarization diminishes the effective salt gradient and leads to a significant drop in power conversion efficiency. <sup>10, 19</sup>

In this manuscript we provide an understanding of how pore length affects ion conductance in single nanopores and small 3-nanopore arrays as a function of pore length, surface charge, and voltage. Specifically, we provide guidelines on how to maximize conductance and ion selectivity. We consider cylindrically shaped nanopores with a pore opening of 5 nm in diameter located 15 nm away from each other. The pore walls are charged while the membrane surfaces remain uncharged. We present surprising results that point to the existence of a range of pore lengths where the ionic conductance at low voltages is independent of the pore length. The findings are explained by ion concentration polarization<sup>20-23</sup> that changes local ionic concentrations at the pore entrance as well as in the pore, and can affect ion selectivity of single pores and arrays.<sup>19, 23, 24</sup> Results with homogeneously charged pores are contrasted with pores that contain a junction between zones with positive and negative surface charges.<sup>25, 26</sup> The manuscript also provides approaches to quantify the size of the depletion zone caused by ion concentration polarization. The modeling shown here will help design selective nanopores for a variety of applications where single nanopores and arrays are used.

### **Methods**

## **COMSOL** finite element analysis simulations

lonic transport in single nanopores and 3 - nanopore arrays with pores of varying length was modeled using the coupled Poisson-Nernst-Planck equations (1-2) solved with COMSOL Multiphysics.

$$-\epsilon_f \nabla^2 \varphi = \sum_{i=1}^2 F z_i c_i \tag{1}$$

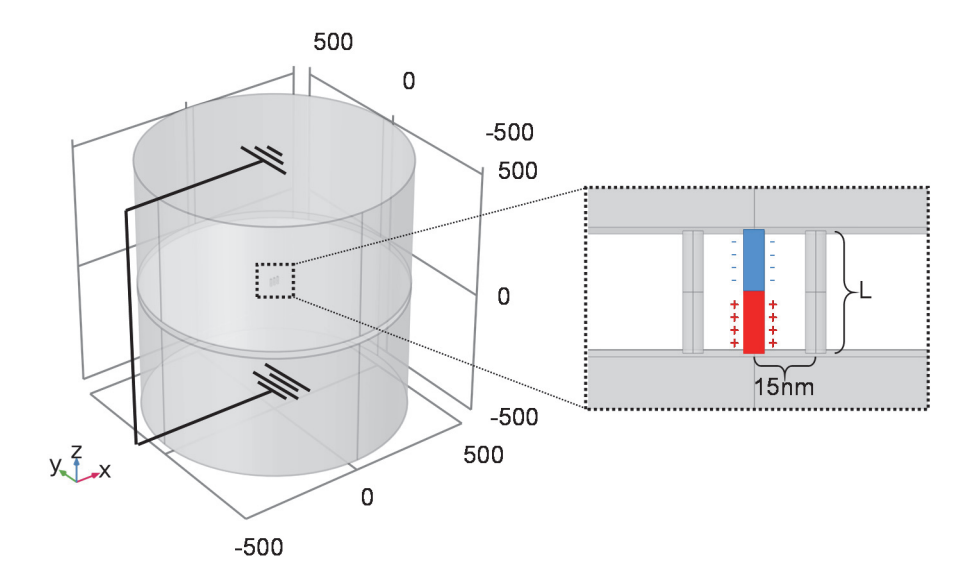
$$\nabla \cdot J_i = \nabla \cdot \left[ -D_i \nabla c_i - \frac{z_i F}{RT} D_i c_i \nabla \varphi \right] = 0$$
 (2)

Table 1: Description of variables used in COMSOL simulations

Variable	Description
φ	Electric potential
$J_i$	Flux of $i^{th}$ ionic species
$c_i$	Concentration of <i>i</i> <sup>th</sup> ionic species
$D_i$	Diffusivity of $i^{th}$ ionic species, $2 \cdot 10^{-9}$ m <sup>2</sup> /s for K <sup>+</sup> and Cl <sup>-</sup>
$z_i$	Valence of <i>i</i> <sup>th</sup> ionic species
F	Faraday constant
$\epsilon_f$	Fluid permittivity, 80
R	Gas constant
T	Absolute temperature

Three-dimensional models were considered due to lack of axial symmetry of the nanopore arrays. Including the Navier Stokes equations had negligible effects on results and substantially increased the time of convergence and were therefore omitted.<sup>27</sup> Note that the model does not consider ions that can adsorb to the pore walls and change the effective surface charge density and selectivity.<sup>28</sup>

The basic structure of all models consisted of a single cylindrical nanopore or 3-nanopore array embedded between two cylindrical reservoirs with a radius and height of 0.5 µm each (Figure 1).<sup>29</sup> Individual nanopores were constructed with opening diameters of 5 nm and varying pore lengths of 5, 10, 20, and 30 nm. Pore to pore distance in arrays was measured from the center of a given nanopore to the center of the neighboring pore and was set to 15 nm. A potential sweep was applied from -2 V to 2 V with a step of 0.2 V, and in some cases 0.1 V. Figure 1 details the surfaces where the potential and bulk concentrations were declared in the model. We used KCl concentrations of 10 mM, 100 mM, and 1 M with a diffusion coefficient of 2·10-9 m²/s for each species. Two types of nanopores with different surface charge distributions were considered: homogenously charged nanopores with charge density of -0.05 C/m², and nanopores containing a junction between positively (0.05 C/m²) and negatively (-0.05 C/m²) charged zones of equal length.



**Figure 1. Geometrical setup for nanopore array modeling.** Cylindrical reservoirs of  $0.5~\mu m$  radius and  $0.5~\mu m$  height are connected with a membrane containing a single nanopore or 3-nanopore array with the pore-to-pore distance set to 15~nm. The nanopore diameter was 5~nm in all simulations, while the pore length, L, was varied between 5~nm and 30~nm. Blue and red regions indicate negatively and positively charged pore walls, respectively.

### **Results and Discussion**

Transport properties of individual nanopores and arrays of nanopores with surface charges are affected by ion concentration polarization (ICP).<sup>20-23, 30</sup> When an electric potential difference is applied, a depletion zone is created on one side of the membrane, and a zone with enhanced concentration of ions on the other side of the membrane. When nanopores are located close to each other, the depletion zones of neighboring nanopores overlap and limit the current through the array.<sup>23, 29-32</sup> Here we look in detail how the pore length influences concentration polarization and current through a 3-nanopore array where the pores are located 15 nm away from each other.<sup>29</sup> Four nanopore lengths are considered, 5 nm, 10 nm, 20 nm, and 30 nm while keeping the pore diameter constant at 5 nm. We aim at identifying geometric and surface charge conditions that will assure maximum current and ion selectivity. Results for the array are compared with predictions for single nanopores. We first present results for nanopores whose walls are negatively charged, followed by analysis of nanopores containing a junction between a zone with negative surface charges and a zone with positive surface charges.

## lon concentration polarization leads to unusual dependence of the pore conductance and selectivity on pore length, voltage, and salt concentration.

Transport properties of nanopores with surface charges have to be considered together with the adjacent reservoirs, where local ionic concentrations are modulated by the ICP.<sup>21, 29, 33</sup> We begin, therefore, with the analysis of ionic depletion that is created by the applied voltage at one pore opening. Figure 2 shows surface concentration maps of single nanopores (Figure 2 a-d) and 3-nanopore arrays (Figure 2 i-l) in 100 mM KCl. These maps are in a plane at 5 nm distance to the membrane surface on the side of the membrane that is kept at a positive potential, thus where

we expect the depletion zone to form. Results in 10 mM and 1 M KCl are shown in Figures S1, S2. The heat maps were created at 2 V and confirm that in arrays there is a significant overlap of depletion zones of neighboring pores (Figure 2 i-l).<sup>23</sup> In order to understand how ionic concentrations at pore entrances for pores of different lengths are affected by the applied voltage, Figure 2 e-h (Figure 2 m-p) shows the total ionic concentration along the white dashed line indicated in panels a-d (i-l) for single nanopores (3-nanopore arrays). Voltages between 0 V and 2 V with 0.1 V step were considered. As expected,<sup>23, 29, 31, 32</sup> the concentration at the pore entrances is strongly affected by the applied voltage, and the depletion zone is more pronounced (both in width and in minimum concentration) for the arrays than for the single nanopores.<sup>29</sup>

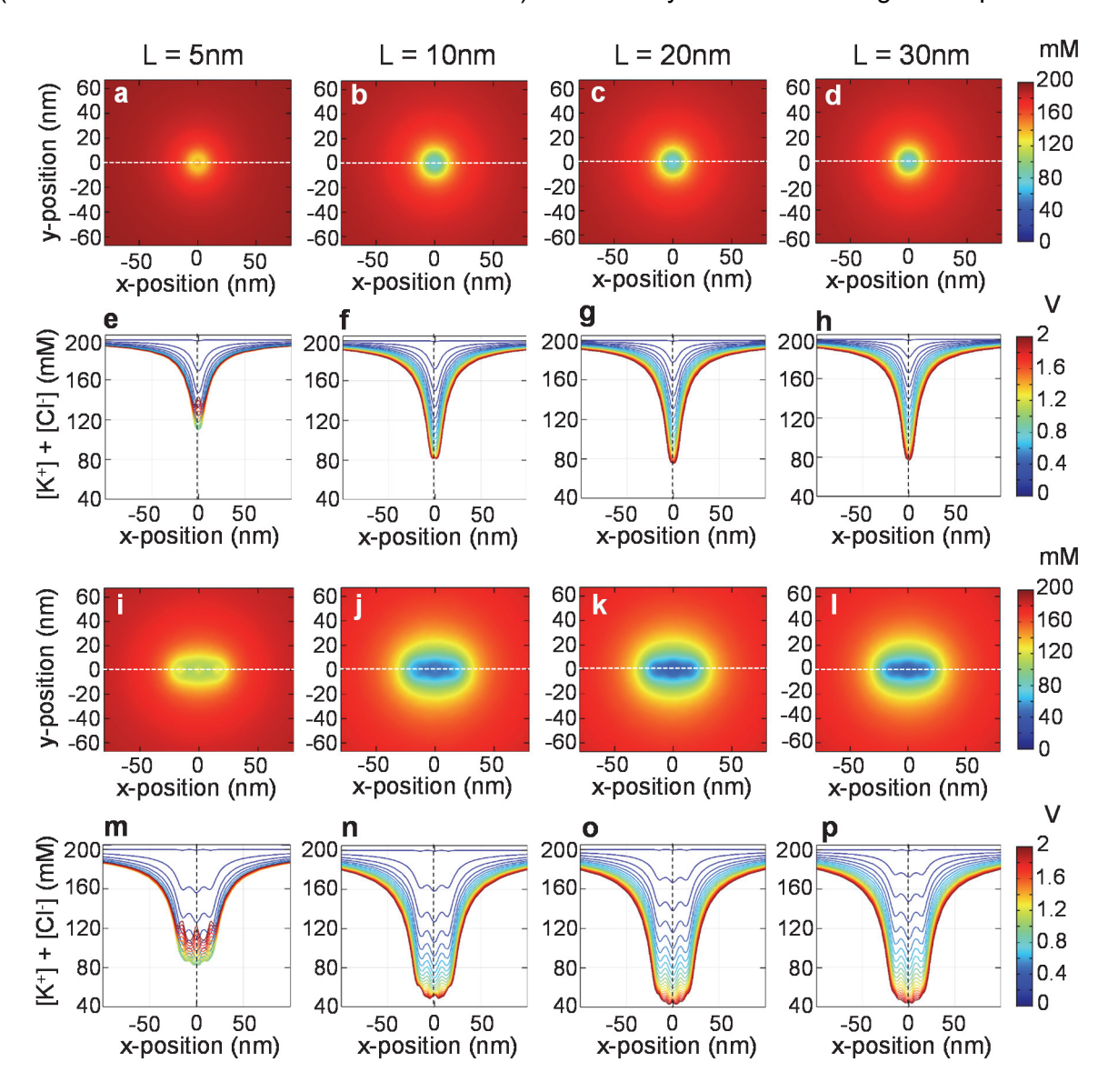


**Figure 2**. Ionic depletion caused by ion concentration polarization in single nanopores (a-h) and in nanopore arrays with 3 pores (i-p) in 100 mM bulk KCl concentration as a function of pore length and voltage. Results for 5, 10, 20, and 30 nm long pores are shown in subsequent columns from left to right. All nanopores had a surface charge density on the pore walls of -0.05 C/m<sup>2</sup>. The depletion is formed on the side of the membrane that is the source of cations i.e. the side kept at

positive potential. (a-d) and (i-l) show surface heat maps at 2 V of the total concentration of  $K^+$  and  $Cl^-$  at a distance 5 nm away from the membrane surface for single pores and arrays, respectively. (e-h) and (m-p) show ionic concentrations along the dashed horizontal line in the heat maps as a function of transmembrane potential between 0 V and 2 V for single nanopores and arrays. For all arrays an interpore spacing of 15 nm from center to center was used with the center pore located at (0,0,0).

The data in Figure 2 were further analyzed to understand the degree of ionic depletion in pores of different lengths as a function of salt concentration and voltage. We considered all single pores and arrays, and in Figure 3 we plot the concentration at the pore axis at a distance of 5 nm to the membrane, as designated in Figure 2 by black dashed vertical lines, for 10 mM, 100 mM, and 1 M. This concentration, called here  $c_{\text{dep}}$ , offers a simplified measure of the degree of ionic depletion. We begin by describing the results in 10 mM KCl, where the depletion zones for all arrays and single nanopores at voltages below 0.5 V are nearly pore-length independent (Figures S1, 3a). There is only a very weak decrease of the concentration,  $c_{\text{dep}}$ , with a decrease of pore length for low voltages (up to ~0.2 V), which can be understood by the stronger electric field achieved in shorter pores for the same voltage, leading to stronger ionic depletion. For voltages above 0.6 V, the arrays with 10 nm – 30 nm long pores feature a nearly identical  $c_{\text{dep}}$  that is only weakly voltage dependent. In contrast, for the 5 nm pore, an increase of  $c_{\text{dep}}$  with voltage is observed above 0.6 V. The results suggest that there is a voltage threshold for shorter nanopores beyond which ion current polarization is weakened, possibly due to a weakened ionic selectivity. This hypothesis is discussed below.

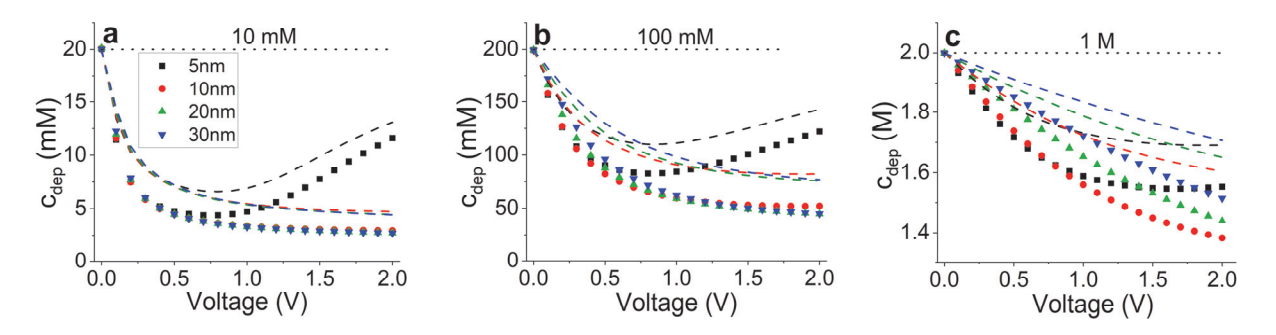


**Figure 3**. Total ionic concentration,  $c_{dep}$ , in the depletion zone just outside of single nanopores (dashed lines) and the center pore in the arrays (symbols), as a function of pore length and voltage. This graph shows concentrations at the pore axis at a distance of 5 nm to the membrane (vertical dashed lines shown in Figure 2 (e-h) and (m-p)). This concentration is treated as a measure of the degree of ionic depletion. The dotted horizontal lines show total bulk concentration of ions.

In 100 mM KCI (Figure 3b), for voltages below 0.3 V, the pore length affected  $c_{dep}$  to a larger extent than seen in 10 mM KCI. In the low-voltage range, up to ~0.2 V, similar to what we observed in 10 mM, the concentration  $c_{dep}$  was lower for shorter pores, in line with the expectation that the same voltage creates a higher electric field in shorter pores and thus a stronger depletion. As observed in 10 mM KCI (Figure 3a), in 100 mM the 5 nm long pores also behave differently than

the longer pores, and for voltages above 0.8 V, an increase in  $c_{dep}$  with voltage is observed. Finally, in 1 M KCI (Figure 3c),  $c_{dep}$  decreased with a decrease of the pore length, however, as expected, the depletion was significantly weaker compared to what we observed in 10 mM and 100 mM, with  $c_{dep}$  reaching ~70% of the bulk concentration. Interestingly, the 5 nm long pores still exhibited saturation of  $c_{dep}$  with voltage at ~ 1.5 V, and we have verified numerically that above 2 V,  $c_{dep}$  again increases with voltage (not shown). Voltages beyond 2 V were not considered in detail for other cases, because they would create sufficiently high electric fields to cause dielectric breakdown of common membrane materials such as silicon nitride and silica.  $^{34, 35}$ 

The analysis of the depletion zone at the pore entrance has revealed a non-trivial dependence of local ionic concentration on pore length, voltage and bulk ionic concentration. In the next step, we looked closely at how the formation of the depletion zone influences ion transport through single nanopores and arrays. Figure 4 shows calculated I-V curves for all four considered lengths of single nanopores and nanopore arrays, in 10 mM, 100 mM, and 1 M KCl. The most surprising observation is the lack of dependence of ionic current on pore length at certain conditions. In 10 mM KCI (Figure 4a,d), currents are almost indistinguishable for 10 nm, 20 nm, and 30 nm long pores. And in the small voltage regime of -0.5 V to +0.5 V, all nanopores, even the 5 nm length pore, had nearly identical currents. Note that in 10 mM KCl for low voltages, the depletion zones of all pores considered here were nearly the same (Figure 3a), which could be responsible for their similar conductance. Only at voltages above 0.5 V, 5 nm long nanopores exhibited significantly higher currents than the remaining nanopores, in line with the least pronounced depletion zone at higher voltages (Figure 3a).<sup>12</sup> In 100 mM KCl (Figure 4b,e), currents across 10 nm, 20 nm, and 30 nm pores are very similar to each other, and again the 5 nm pores exhibit the highest conductance. In 1 M KCI (Figure 4c,f), all I-V curves become linear, confirming that the effects of concentration polarization on conductance at this concentration are minimized.

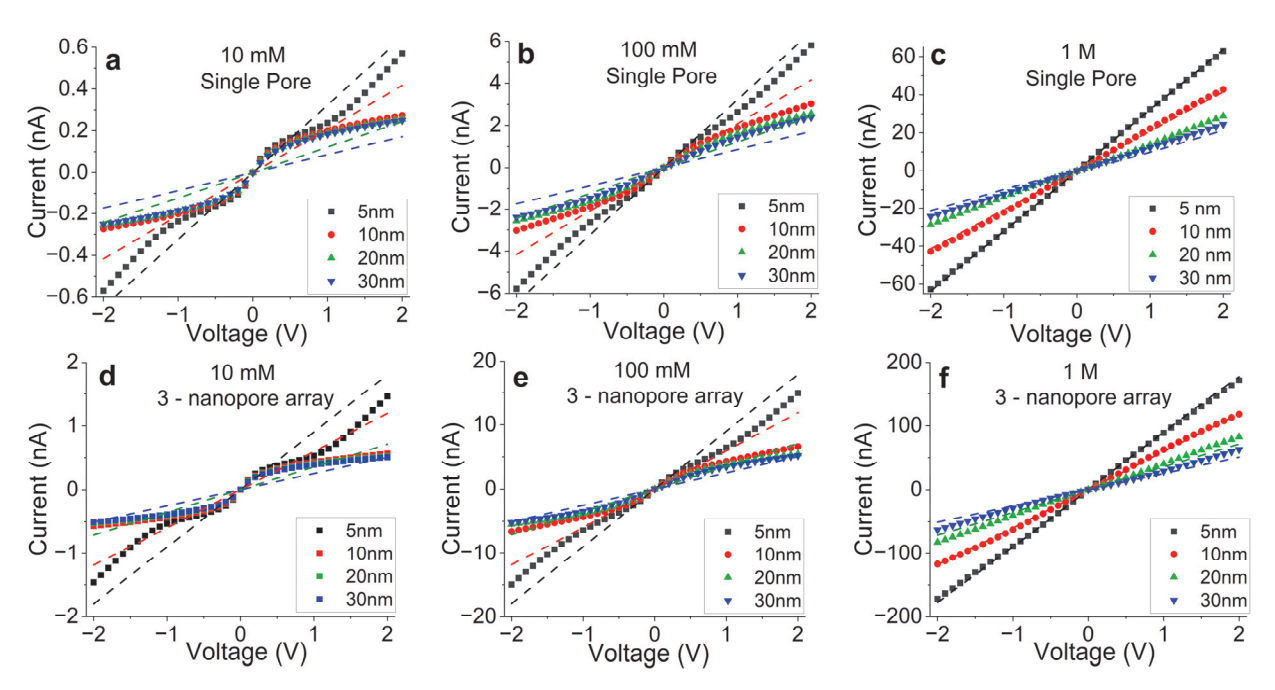


**Figure 4**. Current-voltage curves for single nanopores (a-c) and 3-nanopore arrays (d-f) as a function of bulk salt concentration and pore length. Curves with symbols were obtained for negatively charged nanopores/arrays with -0.05 C/m<sup>2</sup> on the pore walls. Dashed lines represent

current-voltage curves of uncharged pores of the same length as indicated by the color in the legend. The legend indicates the pore length.

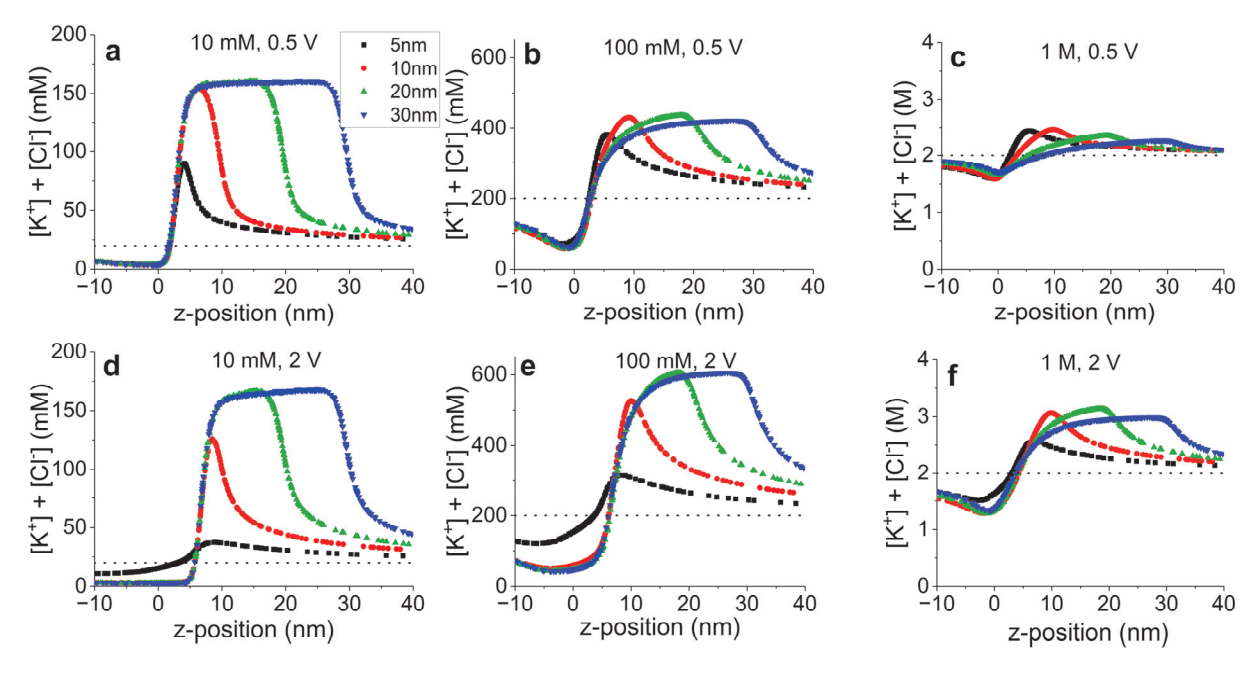
The result on lack of dependence of the current on pore length in low KCI concentrations is surprising, because increasing the pore length, L, is expected to increase the pore resistance that can be calculated as: $^{5, 29, 36, 37}$ 

$$\Omega_{pore} = \Omega_{geom} + \Omega_{access} = \frac{1}{\kappa} \frac{L}{\pi \left(\frac{D}{2}\right)^2} + \frac{1}{\kappa} \cdot \frac{1}{D} \quad (3)$$

where  $\kappa$  is the conductivity of the medium in the pore and D is the pore diameter. Changing the pore length e.g. from 10 nm to 30 nm for 5 nm in diameter pores is expected to increase the pore resistance by a factor of 2.4. If we assume that the transmembrane potential decays primarily over the pore and not in the bulk, the current is expected to decrease by the same factor. Consequently, when we increase the pore length from 5 nm to 10, 20, and 30 nm, the current should decrease by a factor of 1.4, 2.4, and 3.8, respectively. Yet, even in 1 M KCl, where the effects of ICP are minimized, the current in 5 nm long pores is only ~2.6 higher than the current for 30 nm long pores, suggesting that the relatively weak depletion zone at this concentration (Figures 3, S2) can modulate the current.

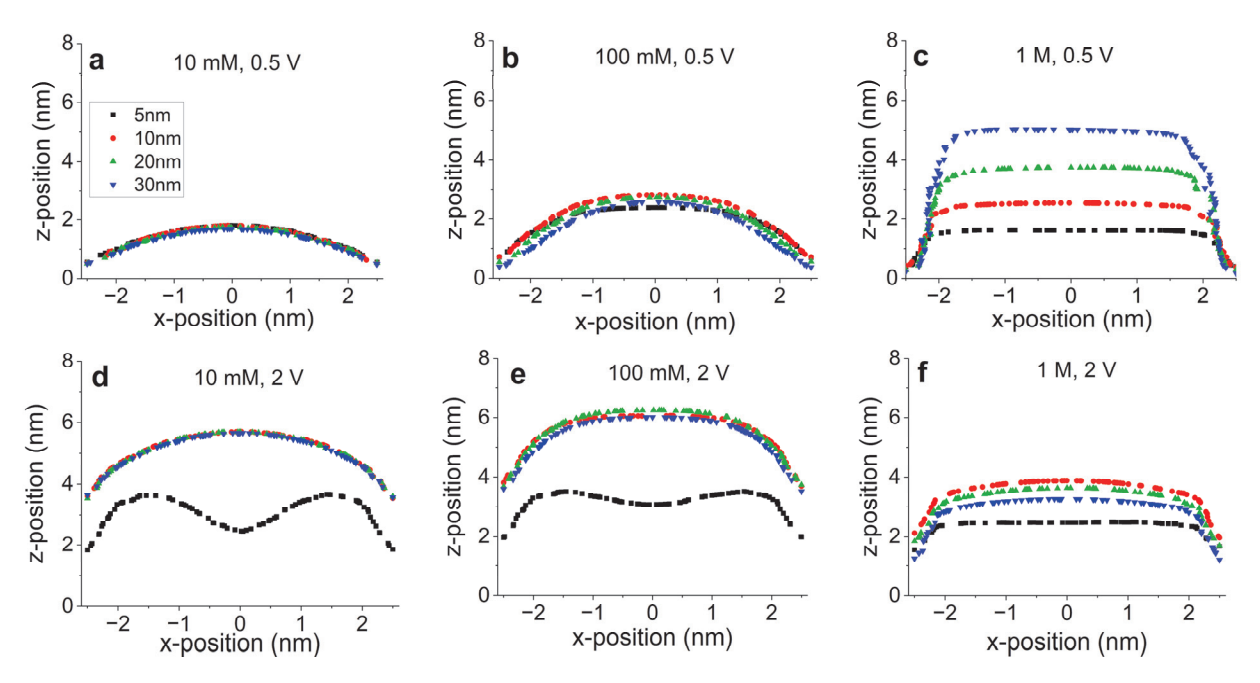
In order to understand at which pore length, L, the pore conductance follows the dependence on L, as predicted by eq. (3), we performed additional numerical modeling of ion current for single nanopores and arrays with a length up to 100 nm. The pores also carried a negative surface charge of -0.05 C/m² on their inner walls. Figure S3 shows ion current at 1 V in 10 mM, 100 mM, and 1 M KCl predicted by the numerical modeling, together with currents calculated using eq. (3) with bulk values of ionic conductivities,  $\kappa$ , for 10 mM, 100 mM and 1 M KCl. We noticed that in 10 mM KCl, in the examined range of pore lengths, the current never reached the expected dependence on L. In 100 mM KCl, the conductance of single nanopores and arrays also decays less slowly with L than predicted by eq. (3). Finally, at 1 M KCl, the currents for single nanopores and arrays are well described by eq. (3) with  $\kappa$  of bulk 1 M solution, confirming ICP is very weak in the system.

Figure 4 also shows I-V curves for pores of different lengths assuming the pore walls are uncharged. It has been shown previously that the presence of surface charges typically enhances ion current, with higher enhancement factors at lower salt concentrations.<sup>1, 4-6, 29</sup> Our modeling showed that nearly at all voltages, 20 nm and 30 nm long pores with surface charges were more conductive than uncharged pores of the same length. On the other hand, surface charges in 5 nm and 10 nm long pores enhanced transport only at low voltage magnitudes, e.g. below 0.5 V and below 0.3 V at 10 mM for 5 nm long single nanopores and arrays, respectively, beyond which the effects of concentration polarization caused the current to be lower than for uncharged pores. Modeling of ion current in 10 mM for voltages above 2 V, up to 5 V, revealed that charged 5 nm long pores were still less conductive than uncharged ones (not shown).



**Figure 5**. Total ionic concentration along the pore axis for the center pore in 3-nanopore arrays as a function of pore length and salt concentration at 0.5 V (a-c) and at 2 V (d-f). Blue, green, red, and black symbols indicate pores that are 30 nm, 20 nm, 10 nm, and 5 nm long. Entrance to all pores is at z = 0 nm. The depletion zone is created at negative z positions where the positive voltage is applied. The dotted horizontal line shows the total bulk concentration of ions.

In order to understand the origin of the pore-length-independent currents in 10 mM KCl in charged nanopores as well as suppression of currents for short nanopores, we examined concentrations of ions in the pore as a function of pore length, voltage and salt concentration. Figure 5 shows profiles of total ionic concentrations along the pore axis at two voltages (0.5 V and 2 V). Results for the center pore in 3-nanopore arrays are shown. The profiles clearly reveal that the depletion zone created at the pore entrance extends into the pore volume<sup>29, 38</sup> and is followed by a region with significantly enhanced ionic concentration. Quantitatively similar observations were made for all concentrations, with the weakest depletion/enhancement in 1 M KCl, as expected. We predicted that the presence of the depletion zone at the pore entrance and in the pore controls the pore conductance and is responsible for the weak dependence of conductance on pore length.



**Figure 6**. Contours of the position in the xz-plane inside the pore where the total ionic concentration reaches 95% of the bulk total concentration. x = 0 nm indicates the middle of the center pore in 3-nanopore arrays of all lengths. The vertical axis indicates the position along the pore axis (z-direction) away from the entrance with the depletion zone.

To quantify the length of the zone in the pore with depleted concentrations, we found the position along the pore axis (z-direction) where the concentration reaches 95% of the total ionic bulk concentrations (i.e., 20 mM, 200 mM, and 2000 mM). Figure 6 shows this location in the xdirection, creating a contour plot that provides a measure of the depth of the depletion zone in a pore. In 10 mM KCl and 0.5 V, the extent of the depletion zone for all pores is nearly the same (Figure 6a). In addition, we hypothesize that the remaining part of the pore contributes to the total resistance in a negligible way, because it is filled with solution of significantly higher concentration than the bulk (enhancement by a factor of ~4 for the 5 nm long pores and a factor of ~8 for 10 -30 nm long pores, Figure 5). To support this hypothesis, we determined how much of the applied transmembrane potential,  $\Delta V_{transmembrane}$ , drops over the depletion zone. To this end, for each  $\Delta V_{transmembrane}$ , we determined voltage drop,  $\Delta V_{depletion}$  that occurs over the region where the ionic concentration is below 95% of the bulk concentration. The resulting ratio,  $\Delta V_{\text{depletion}}/\Delta V_{\text{transmembrane}}$ , informs us on the fraction of  $\Delta V_{transmembrane}$  that drops over the depletion zone (Figure 7). Figure 7a shows that in 0.5 V and 10 mM KCl, ~90% of the voltage drop occurs over the depleted region. These results demonstrate that in 10 mM KCl and at low voltages, the effective lengths of the 5-30 nm long pores, determined by the extent of the respective depletion zone, are identical, leading to nearly identical currents.

Once the voltage increases to 2 V, the extent of the depletion zone in the pores in 10 mM KCl is larger than at the lower voltage but remains the same for 10-30 nm long pores (Figure 6d). Ion concentrations in the depletion zones (and in the enhancement zones) are also nearly independent of the pore length (Figure 5). Consequently, for 10-30 nm long pores in 10 mM KCl, again the majority (over 90%) of the transmembrane potential drops over the depletion zone at the entrance and in the pore (Figure 7a), leading to pore-length-independent ion currents. The

extent of the depletion zone in 5 nm long pores, however, is smaller than in the longer pores (Figure 6d). Moreover, ionic concentrations in the whole volume of the 5 nm long pores are closer to the bulk than it was observed in 0.5 V (Figure 5 a,d), suggesting that the pore became less ion selective. Consequently, the region with concentrations below 95% of bulk creates a smaller resistive component, such that the ion current is overall significantly higher than for the longer pores.

In 100 mM KCl and 0.5 V (Figure 6b), the extent of the depletion zone is larger than in 10 mM KCI, but again remains nearly identical for all considered pore lengths. The degree of ionic depletion is, however, not as pronounced as in 10 mM KCl, namely the lowest magnitude of concentration at the depletion zone is ~50 mM for the arrays, i.e. 25% of the bulk concentration (Figure 5b), while in 10 mM KCl, the lowest concentration was ~3 mM (~15% of the bulk value). The ionic concentration enhancement in the remaining part of the pore in 100 mM is not as strong either (enhancement by a factor of ~2, Figure 5b), and consequently it will contribute to the total system resistance (Figure 7b). In 100 mM KCl at low voltages, currents for shorter pores are therefore a little higher than for longer pores. As the voltage increases, the depletion and enhancement of ionic concentrations become more pronounced (Figure 5e), and at 2 V the depletion extends deeper into the pore (Figure 6e), compared to what we observed at 0.5 V. The situation is similar to what we saw in 10 mM KCl, and the currents through 10-30 nm long pores are close in magnitude (Figure 4e) with the majority of the voltage drop occurring over the depletion zone (Figure 7b). The 5 nm pores in 100 mM KCl and at higher voltages again conduct more current than the longer pores, in accordance with a less pronounced depletion zone at the pore entrance and in the pore (Figure 5, Figure 6e).

Finally, at 1 M KCI, the depletion is very weak such that the whole pore length contributes to the system resistance, leading to intuitive results of longer pores being more resistive (Figure 4). The fraction of voltage that drops over the depletion zone decreases with increasing pore length (Figure 7c). Note that at 1 M KCI, the extent of the depletion zone in the pore is lower at 2 V compared to 0.5 V (Figure 6c,f), which as we show below is related to the decreasing ion selectivity.

Figures 5-7 also explain why shorter pores with surface charges can have lower conductance than equivalent uncharged pores. Note that even though the extent of the depletion zone in the pore is similar in pores of different lengths, it constitutes a different percentage of the overall pore length. In low salt concentrations, a large fraction of short pores is filled with concentrations significantly below bulk, leading to low conductances.

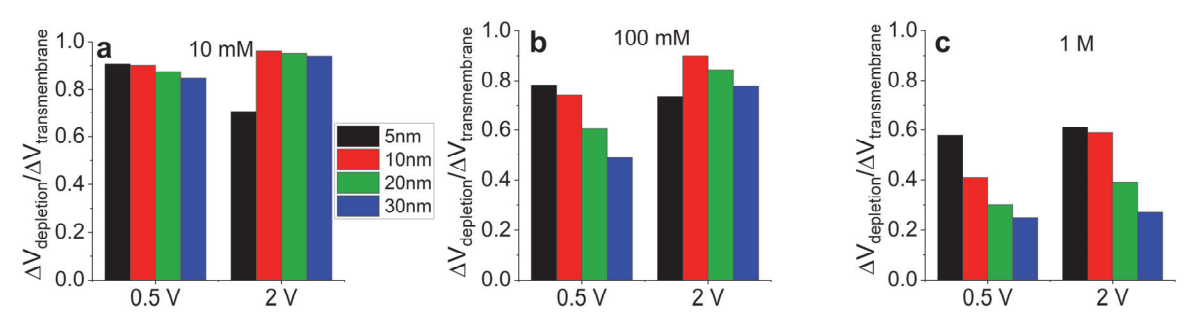


**Figure 7**. Fraction of the transmembrane potential,  $\Delta V_{\text{transmembrane}}$ , that drops over the depletion zone at the pore entrance and in the pore with the voltage drop,  $\Delta V_{\text{depletion}}$ , at two values of

transmembrane potential, 0.5 V and 2 V, in (a) 10 mM, (b) 100 mM, and (c) 1 M KCl as a function of pore length. A ratio  $\Delta V_{depletion}/\Delta V_{transmembrane}$  approaching 1 indicates that the applied voltage drops predominantly over the depletion zone.

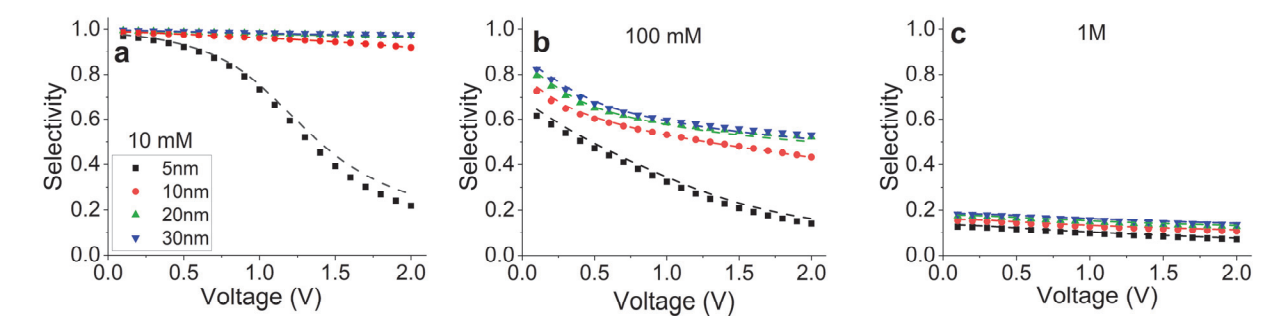


**Figure 8**. Cation selectivity of single nanopores (dashed lines) and 3-nanopore arrays (symbols) as a function of pore length and voltage in (a) 10 mM, (b) 100 mM, and (c) 1 M KCI. Selectivity is calculated as the difference between currents carried by cations and anions, divided by the total ion current, eq. (4).

Figures 2-7 consider total ion concentration together with resulting current and distribution of electric field, but they do not link the observations to the ionic selectivity of the pores. Ion concentration polarization occurs for nanopores that are ion selective, thus we wanted to understand how the formation of the depletion zone and the dependence of ion current on pore length are linked with voltage-dependent cation selectivity. Cation selectivity is defined here as the difference between currents carried by cations,  $I_{K^+}$ , and anions,  $I_{Cl^-}$ , normalized by the total ion current carried by both types of ions:<sup>12</sup>

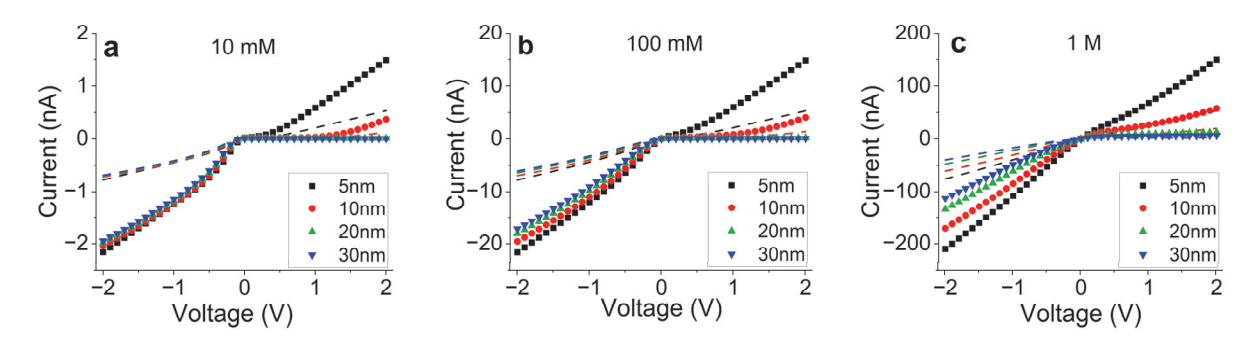
$$Selectivity = \frac{I_{K^{+}} - I_{Cl^{-}}}{I_{K^{+}} + I_{Cl^{-}}}$$
 (4)

Figure 8a shows ion selectivity in 10 mM KCl for all considered pores as a function of voltage. In the low voltage regime, all nanopores are highly cation selective, which is in agreement with the existence of significant and nearly length-independent depletion zones. As the voltage increases, the 5 nm pores become only weakly ion selective that led to the weakened ion concentration polarization and increased currents (Figures 3, 4). In 100 mM KCl (Figure 8b), as expected, the ion selectivity for all pores at all voltages is lower than in 10 mM KCl, but remained nearly the same for the 20-30 nm long pores. Note that the 10-30 nm long pores exhibit similar currents for higher voltages, suggesting that ion selectivity and ICP are key effects responsible for porelength-independent current. It is also important to note that ion selectivity in 100 mM KCl for 10 - 30 nm long pores decays faster with voltage than in 10 mM. In 1 M KCl (Figure 8c), ionic selectivity for all considered nanopores stays below 0.2 and approaches zero at high voltages, leading to weak, although non-zero (Figures 3-7) ICP effects.

Ion concentration polarization and conductance of nanopores with diodes.

Our earlier results suggested that ion concentration polarization can be mitigated by introducing a surface charge pattern on the pore walls, specifically, a junction between a zone with positive surface charges and a zone with negative surface charges.<sup>29</sup> Pores containing such junction are known to behave as ionic diodes, i.e. currents for voltages of one polarity are higher than currents for the opposite voltage polarity.<sup>25, 26, 39</sup> Following our analysis with pores containing only negative surface charges, we wanted to understand the role of the pore length and voltage for ionic conductance of arrays with ionic diodes.

Figure 9 shows current-voltage curves through single ionic diodes and through an array of 3 diodes with an interpore distance of 15 nm. As expected,  $^{39}$  the I-V curves were strongly asymmetric with high rectification degrees in 10 mM and 100 mM KCl for 10 - 30 nm long diodes (Figure 10). Similar to the results with homogeneously charged nanopores, in 10 mM KCl, current-voltage curves for 10 - 30 nm long ionic diodes were almost identical, with the exception of an increased positive current for the 10 nm long nanopore at voltages above 1 V (Figure 9a). Interestingly, the 5 nm long diode showed nearly identical negative currents as the longer pores, but the diode opened up for ionic transport at positive voltages as well, losing its rectification properties at high voltages (Figure 10).



**Figure 9**. Current-voltage curves through single nanopores (dashed lines) and arrays (symbols) that function as ionic diodes. The dependence on pore length and bulk salt concentration is shown: (a) 10 mM, (b) 100 mM, and (c) 1 M. The pores have a junction between two zones with opposite surface charges.

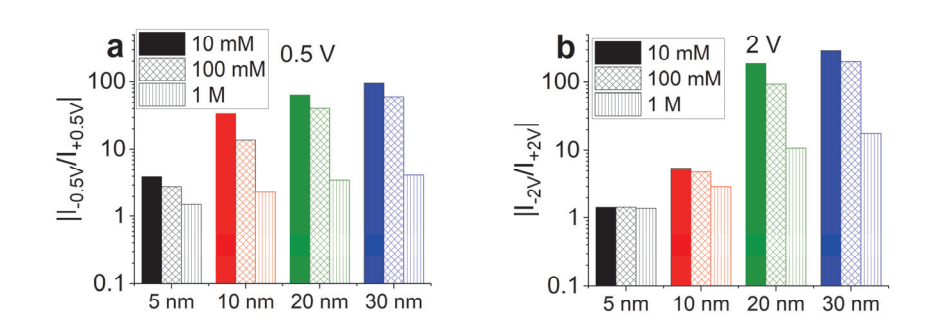


**Figure 10**. Rectification degrees of 3-nanopore arrays containing ionic diodes, calculated based on I-V curves shown in Figure 9 as ratios of currents at (a) -/+ 0.5 V, and (b) -/+ 2 V. Rectification for diodes that are 5 nm, 10 nm, 20 nm, and 30 nm long is shown.

In order to understand if concentration polarization is also responsible for the weak dependence of the conductance of ionic diodes on pore length, we looked at the distribution of total ionic concentration along the pore axis, including the reservoirs regions, as performed in Figure 5 for negatively charged pores. Results for -0.5 V and -2 V, corresponding to the 'on', high conductance state of the system of 3 ionic diodes are shown in Figure 11, while the equivalent distributions for positive voltages are shown in the Supporting Information (Figure S4).

In contrast to pores with negative surface charges, there is an insignificant concentration polarization at the pore entrances in the reservoirs, such that the pore entrances are in contact with a solution of nearly bulk concentration for both 'on' and 'off' states (Figure 11a-f, Figure S4a-f). The transmembrane voltage causes however an enhancement of ionic concentration in the pore for negative voltages (Figure 11), and a depletion for positive voltages (Figure S4) in the region of the junction between zones with positive and negative surface charges. Here, we will describe in detail the distributions of ionic concentrations for negative voltages.

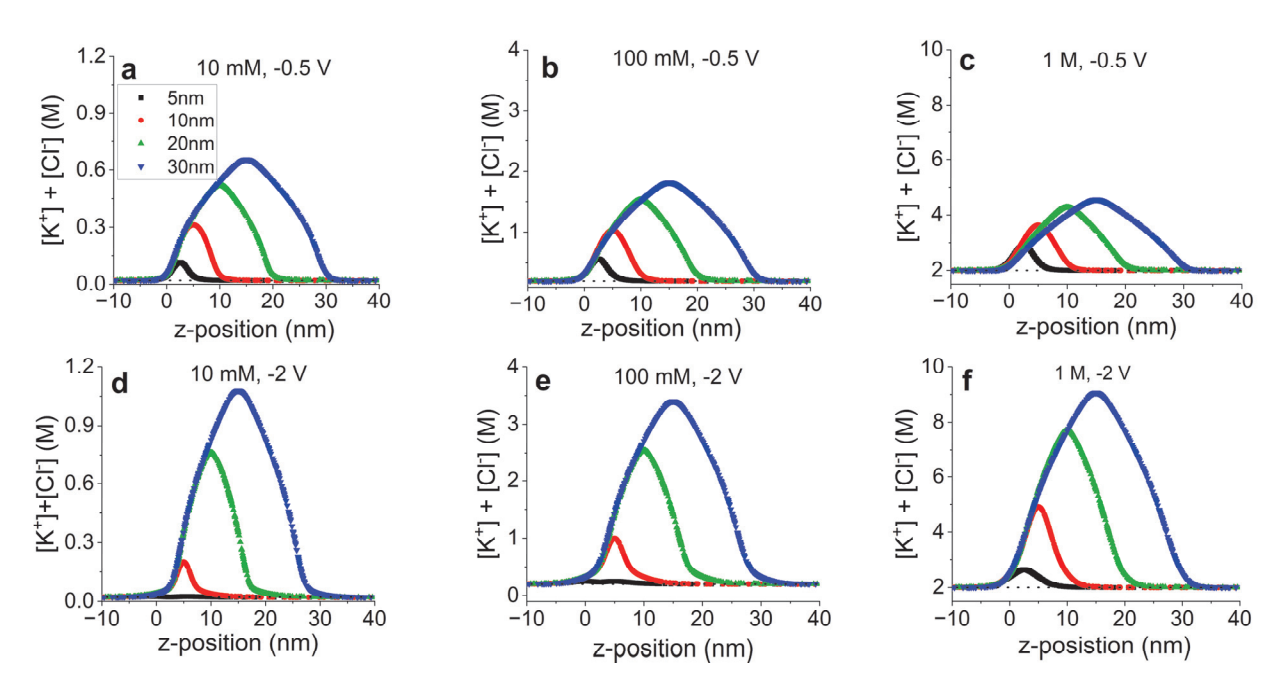


**Figure 11**. Total ionic concentration along the pore axis for the center pore in 3-nanopore arrays containing ionic diodes at -0.5 V (a-c) and at -2 V (d-f). *Entrance to all pores is at z = 0 nm. The dotted horizontal line shows total bulk concentration of ions. Ionic concentrations at +0.5 V and +2 V are shown in Figure S4.* 

The ionic enhancement strongly depends on the magnitude of negative transmembrane potential, and increases with an increase of the pore length (Figure 11). In 10 mM KCl and -0.5 V, the highest concentration for 30 nm long nanopores is ~5.5, ~2.1, and ~1.3 times larger than the highest concentration for 5 nm, 10 nm, and 20 nm long pores, respectively. Consequently, resistance decrease due to the concentration enhancement and resistance increase due to increased length cancel out, and at 0.5 V, diodes of all lengths conduct the same amount of current (Figure 9a). At -2 V, 10 mM KCl, even though the concentration in the 5 nm long

nanopores decreases due to decreased ionic selectivity in the two zones, the short diodes still conduct the same amount of current as the long diodes (Figures 9a, 11d). In 100 mM KCI (Figure 11b,e), ionic concentration in the pore increases with voltage only for 20 nm and 30 nm long nanopores, but again the enhancement is significantly strong for all pores such that similar conductances at negative voltages are observed for diodes of all lengths. Even in 1 M KCI (Figure 11c,f), ionic concentrations are modulated by voltage leading to currents that are more similar for diodes of different lengths than one could predict based on geometrical characteristics of the pores. Modulation of ionic concentrations in all nanopores explains the presence of ion current rectification even in 1 M KCI. Note that total ionic concentrations in diodes exceed ionic concentrations in negatively charged pores (Figure 5), due to enhanced concentrations of positive and negative ions in nanopores containing a diode junction. The modeling predicted ionic concentrations reaching 9 M in 1 M KCI bulk solution at -2 V, which is likely unphysical due to limited solubility of the salt. This large increase of ionic concentrations in 1 M KCI stems from the assumption of the continuum model on the point charge character of ions and is not expected in experiments.

The ion depletion zone in the diodes created at positive voltages is also highly dependent on pore length, salt concentration, and voltage (Figure S4). 20 nm and 30 nm long diodes exhibit most pronounced depletion zones that led to the lowest positive currents, and highest rectification degrees. 5 nm long diodes exhibit the highest concentration in the pore in the 'off' state and consequently they rectify the least.

The modeling with diodes revealed that the ionic depletion present at one pore entrance of homogeneously charged nanopores is not present for diodes. Instead, pore-length, voltage and salt concentration modulate local ionic concentrations inside the volume of ionic diodes. 5 nm long pores with negative surface charges and 5 nm long diodes lose their ionic selectivity at higher voltages, leading to weaker modulation of ionic concentrations.

#### Conclusions

lonic transport through nanopores with charged walls can be strongly affected by the concentration polarization that modifies ionic concentrations not only at the pore entrance but also in the pore. The extent of concentration polarization in the pore volume is especially important for low-aspect-ratio pores where the regions with depleted concentration can fill a significant portion of the pore volume, leading to pore-length independent conductance in low salt concentrations. Our results suggest that thick membranes can exhibit the same conductance as several times thinner membranes suggesting there is an optimal set of geometric and electrochemical properties of nanopores that maximize conductance and selectivity. The range of pore lengths with nearly identical conductance was observed for single nanopores and arrays, however the effect was more pronounced for the arrays. The numerical models also demonstrated that even though concentration polarization poses limits to ionic conductance of porous media, modulating surface charge patterns can affect where ionic depletion/enhancement is formed and thereby tune transport properties of nanopores. For ionic diodes, ionic enhancement or depletion is created inside the pore such that both entrances of the pores are in contact with bulk solution for all pore lengths, voltages, and salt concentrations studied. Consequently, even 5 nm long nanopores containing a junction between oppositely charged zones rectify the current at low voltages. This study is important for designing separation membranes that feature high flux and selectivity as well as membranes for blue energy conversion. The reported 3D modeling also enables

visualization and quantification of ion depletion and enhancement zones induced in nanopores by ICP.

### Conflict of Interest

The authors declare no conflict of interest.

## **Acknowledgments**

The work was funded by the National Science Foundation CHE, MPS 2200524.

## References

- 1. R. B. Schoch, J. Y. Han and P. Renaud, *Rev. Mod. Phys.*, 2008, **80**, 839-883.
- 2. H. Daiguji, P. Yang and A. Majumdar, *Nano Lett.*, 2004, **4**, 137-142.
- 3. D. Stein, M. Kruithof and C. Dekker, *Phys. Rev. Lett.*, 2004, **93**, 035901.
- 4. A. Plecis, R. B. Schoch and P. Renaud, *Nano Lett.*, 2005, **5**, 1147-1155.
- 5. C. Lee, L. Joly, A. Siria, A.-L. Biance, R. Fulcrand and L. Bocquet, *Nano Lett.*, 2012, **12**, 4037-4044.
- 6. Y. Green, J. Chem. Phys., 2021, 154, 084705.
- 7. S. Su, Y. Zhang, S. Peng, L. Guo, Y. Liu, E. Fu, H. Yao, J. Du, G. Du and J. Xue, *Nat. Commun.*, 2022, **13**, 4894.
- 8. Z. Zhu, D. Wang, Y. Tian and L. Jiang, J. Am. Chem. Soc., 2019, **141**, 8658-8669.
- 9. S. Zhang, J. Wang, A. Yaroshchuk, Q. Du, P. Xin, M. L. Bruening and F. Xia, *J. Am. Chem. Soc.*, 2024, **146**, 11036-11042.
- 10. L. Cao, Q. Wen, Y. Feng, D. Ji, H. Li, N. Li, L. Jiang and W. Guo, *Adv. Funct. Mater.*, 2018, **28**, 1804189.
- 11. L. Ma, Z. Li, Z. Yuan, H. Wang, C. Huang and Y. Qiu, *J. Power Sources*, 2021, **492**, 229637.
- 12. I. Vlassiouk, S. Smirnov and Z. Siwy, *Nano Lett.*, 2008, **8**, 1978-1985.
- 13. J. D. Feng, M. Graf, K. Liu, D. Ovchinnikov, D. Dumcenco, M. Heiranian, V. Nandigana, N. R. Aluru, A. Kis and A. Radenovic, *Nature*, 2016, **536**, 197-200.
- 14. A. Siria, P. Poncharal, A. L. Biance, R. Fulcrand, X. Blase, S. T. Purcell and L. Bocquet, *Nature*, 2013, 494, 455-458.
- 15. M. Tsutsui, W.-L. Hsu, D. Garoli, I. W. Leong, K. Yokota, H. Daiguji and T. Kawai, *ACS Nano*, 2024, **18**, 15046-15054.
- 16. Z. Zhang, L. Wen and L. Jiang, *Nat. Rev. Mater.*, 2021, **6**, 622-639.
- 17. Z. Zhang, L. He, C. Zhu, Y. Qian, L. Wen and L. Jiang, *Nat. Commun.*, 2020, **11**, 875.
- 18. G. H. Xie, L. P. Wen and L. Jiang, *Nano Res.*, 2016, **9**, 59-71.
- 19. L. Wang, Z. Wang, S. K. Patel, S. Lin and M. Elimelech, *ACS Nano*, 2021, **15**, 4093-4107.
- 20. W. Han and X. Chen, J. Chem. Technol. Biotechnol., 2020, 95, 1622-1631.
- 21. Y. Green, S. Shloush and G. Yossifon, *Phys. Rev. E.*, 2014, **89**, 043015.
- 22. T. A. Zangle, A. Mani and J. G. Santiago, *Chem. Soc. Rev.*, 2010, **39**, 1014-1035.
- 23. V. Freger, Faraday Discuss., 2018, **209**, 371-388.
- 24. Z. S. Siwy, M. L. Bruening and S. Howorka, *Chem. Soc. Rev.*, 2023, **52**, 1983-1994.
- 25. Z. S. Siwy and S. Howorka, *Chem. Soc. Rev.*, 2010, **39**, 1115-1132.

- 26. H. Daiguji, Y. Oka and K. Shirono, *Nano Lett.*, 2005, **5**, 2274-2280.
- 27. R. A. Lucas, C.-Y. Lin, L. A. Baker and Z. S. Siwy, *Nat. Commun.*, 2020, **11**, 1568.
- 28. Z. Ni, H. Qiu and W. Guo, J. Phys. Chem. C, 2018, **122**, 29380-29385.
- 29. E. Cao, D. Cain, S. Silva and Z. S. Siwy, *Adv. Funct. Mater.*, 2024, **34**, 2312646.
- 30. S. Liu, X. Zhang, Y. Yang and N. Hu, *Anal. Chem.*, 2024, **96**, 5648-5657.
- 31. Y. Liu, M. Sairi, G. Neusser, C. Kranz and D. W. M. Arrigan, *Anal. Chem.*, 2015, **87**, 5486-5490.
- 32. Y. Liu, A. Holzinger, P. Knittel, L. Poltorak, A. Gamero-Quijano, W. D. A. Rickard, A. Walcarius, G. Herzog, C. Kranz and D. W. M. Arrigan, *Anal. Chem.*, 2016, **88**, 6689-6695.
- 33. Y. Green, R. Abu-Rjal and R. Eshel, *Phys. Rev. App.*, 2020, **14**, 014075.
- 34. H. Kwok, K. Briggs and V. Tabard-Cossa, *Plos One*, 2014, **9**, e92880.
- 35. I. Yanagi, K. Fujisaki, H. Hamamura and K. Takeda, J. Appl. Phys, 2017, **121**, 045301.
- 36. J. E. Hall, J. Gen. Physiol., 1975, **66**, 531-532.
- 37. R. M. M. Smeets, U. F. Keyser, D. Krapf, M. Y. Wu, N. H. Dekker and C. Dekker, *Nano Lett.*, 2006, **6**, 89-95.
- 38. D. V. Melnikov, Z. K. Hulings and M. E. Gracheva, *The Journal of Physical Chemistry C*, 2020, **124**, 19802-19808.
- 39. I. Vlassiouk and Z. S. Siwy, *Nano Lett.*, 2007, **7**, 552-556.